INTERNATIONAL JOURNAL FOR NUMERICAL METHODS IN FLUIDS
Int. J. Numer. Meth. Fluids 2010; **62**:906–926
Published online 25 March 2009 in Wiley InterScience (www.interscience.wiley.com). DOI: 10.1002/fld.2047

Quadratic stochastic estimation of far-field acoustic pressure with coherent structure events in a 2D compressible plane mixing layer

Ph. Druault*,†, M. Yu and P. Sagaut

Institut Jean Le Rond d'Alembert, Université Pierre et Marie Curie—Paris 6, 4 Place Jussieu, Case 162, 75252 Paris Cedex 05, France

SUMMARY

Mathematical tools based on cross correlations between aerodynamic quantities of interest inside the shear flow region and the radiated sound pressure are used to investigate noise generation mechanisms in a plane compressible mixing layer. An original methodology relying on an efficient coupling between proper orthogonal decomposition (POD) and stochastic estimation procedures is developed to analyze the main aerodynamic mechanisms that govern noise production. POD is used to split the instantaneous flow fluctuations as the sum of three components: the large- and small-scale coherent structures (LCS and SCS) and the background quasi-Gaussian fluctuations. Based on this flow partitioning, quadratic stochastic estimation is implemented to estimate the far-field acoustic pressure associated with each flow component. The far field acoustic pressure associated with both LCS and SCS is then investigated. By analyzing the RMS and temporal spectra of the far-field acoustic pressure, it is observed that the SCSs, as defined thanks to the POD basis, are responsible for the main part of the noise emission. Copyright © 2009 John Wiley & Sons, Ltd.

Received 22 July 2008; Revised 11 February 2009; Accepted 15 February 2009

KEY WORDS: aeroacoustic; plane mixing layer; coherent structures; proper orthogonal decomposition; quadratic stochastic estimation; pressure/velocity correlations

1. INTRODUCTION

The analysis of noise generation by unsteady unbounded shear flows has been of great interest since the introduction of the first aircraft jet engines about 50 years ago. Such an analysis began with the pionnering work of Lighthill [1] who developed a theory of aerodynamic noise generation. In his theory, the acoustic source can be related to aerodynamic fluctuations since the far-field pressure is

*Correspondence to: Ph. Druault, Institut Jean Le Rond d'Alembert, Université Pierre et Marie Curie—Paris 6, 4 Place Jussieu, Case 162, 75252 Paris Cedex 05, France.
†E-mail: philippe.druault@upmc.fr

Copyright © 2009 John Wiley & Sons, Ltd.

directly correlated with the time variations of the unsteady flow field. Thus, a challenging scientific problem consists in identifying the essential physical mechanisms involved in the noise production process.

It is worth noting that the very definition of aeroacoustic sources is still a challenging issue. Existing approaches can roughly been grouped into two families. The first family relies on the Navier–Stokes equations, from which a source term for Dalembertian-type wave propagation operators are recovered. The sources are then identified as the source term. The second family is based on statistical analysis of the field, the aeroacoustic source area being defined as the region that exhibits the highest correlation with the acoustic signal. Here, the fundamental equations of fluid mechanics are not used and the causality principle is invoked to select relevant correlations. Both methods have drawbacks and advantages. The former methods yield explicit mathematical definitions for aeroacoustic sources, but can lead to some controversies dealing with the physical meaning of the expressions (e.g. [2–4]) or the relevancy of splitting the source terms into isolated components. The latter is fully general and can be applied to any flow, but does not provide an explicit formula for the sources. Therefore, bridging between instantaneous features of the flow and noise production is more tricky.

To investigate the noise generation mechanism in unbounded shear flows, computational aeroacoustic (CAA) simulations have been intensively used during the last 20 years. These simulations are based either on the direct computation of the sound, performed on a very large computational domain, including the computation of the far-field acoustic pressure, or on hybrid methods based on the coupling between integral acoustic analogies and near-field computation in the acoustic source zone. Quite satisfactory agreements are obtained with both approaches in the case of free shear flows [5–8]. Experimentally, the investigation of the aerodynamic events involved in the noise production process remains very complex. Such an analysis may be performed, thanks to the causality method [9, 10], which relies on the correlation between aerodynamic events and the noise source defined theoritically [1]. A review of the use of the causality method for that purpose can be found in [9, 11, 12] and references therein.

According to the previous results dealing with unbounded free shear flows, several flow contributions have been identified in noise generation mechanisms. It is now well established that an isolated vortical flow structure is not able to generate noise but that the interaction (or the pairing) between vortical flow structures is the dominant aerodynamic mechanism for noise emission in free shear flows [5, 7, 13, 14]. For a turbulent subsonic jet, previous works have also demonstrated that several noise generation mechanisms occur, depending on individual aerodynamic contributions related to the small-scale random eddies and the coherent flow dynamics [12]. Thus, it has been shown that the primary source of noise in a turbulent jet is the low-order structures of the flow [15, 16]. Moreover, based on two-dimensional (2D) and 3D numerical simulations of a compressible plane mixing layer, Babucke *et al.* [13] observed that the emitted sound also depends on the flow nature: the sound generation in two dimensions is dominated by a tonal noise source, while in three dimensions, broad band noise is emitted.

However, as outlined in Bogey and Bailly [11], the main difficulty relies on the extraction of the aerodynamic events that correspond to the theoritical definition of the noise sources. Indeed, it is now well recognized that in turbulent flows, both LCS and background turbulence coexist and interact. Despite the fact that coherent structures in turbulent flow have been studied intensively during the last 30 years, no unique coherent structure definition and no universal mathematical tool to extract these coherent structures from turbulent flows exist. Coherent structures are embedded within a randomly distributed field and their extraction still remains a very difficult task.

Copyright © 2009 John Wiley & Sons, Ltd.

DOI: 10.1002/fld

Another problem is the difficulty in noise source modelling related to each part of a turbulent flow decomposition.

The current investigation aims at showing that an hybrid methodology, which involves both proper orthogonal decomposition (POD) and stochastic estimation (SE), can be used to better understand the relationship between the flow coherent structures and the far-field acoustic pressure. For that purpose, it is proposed to use the correlations between the dynamics of the unsteady coherent structures and the acoustic emission. Bonnet *et al.* [17] were the first to combine linear stochastic estimation (LSE) and POD approaches, introducing the complementary method. They have performed an LSE of the velocity field from the knowledge of selected velocity components obtained from a limited number of X-wires probes. The resulting field was then projected onto the first POD modes. The aim of such a complementary method is to extract coherent structures of the turbulent flow, using POD decomposition and to access their dynamical evolution, thanks to LSE. More recently, several applications using similar combinations (POD and SE) have been performed to investigate the time evolution of the large-scale flow structures from the knowledge of wall pressure signals [18–20]. Then, these works led to propose a mechanism for the wall pressure generation process within the shear layer flow. Moreover, in a turbulent jet, Picard and Delville [21] performed a POD of the instantaneous spatial pressure distribution to hightlight the dominant patterns of pressure in a turbulent jet. These dominant signatures are then used as conditional events to access the time evolution of the flow structure with the use of the LSE procedure.

To the authors knowledge, published works dealing with the coupled approach (POD–SE) address only the estimation of the large-scale structures from the knowledge of selected pressure signals and of spatial correlation between pressure and velocity fields. Here, we propose a new implementation of this coupled approach that is to perform a quadratic stochastic estimation (QSE) of the far-field acoustic pressure from the knowledge of coherent flow structures extracted with POD procedure. First, POD is used to decompose instantaneous turbulent flow field into three components, namely large coherent structures, small coherent structures and a residual quasi-Gaussian (QG) random motion. Second, each component is used as conditional event for the SE of the far-field acoustic pressure. The objective is then to determine which aerodynamic events are involved in the main noise emission process.

This methodology is assessed by using a purely numerical approach. This new approach is applied to a well-known reference shear flow: the 2D plane compressible mixing layer flow that serves as a good 2D near nozzle model of jets at low computational expense. Moreover, the computational domain can be extended to a very large domain so that direct computation of the far-field pressure is possible, allowing for an accurate validation of the coupled approach.

The paper is organized as follows. Details of the computational set-up and the numerical method are displayed in Section 2. POD and QSE tools are described in Section 3. Results of flow splitting are discussed in Section 4, while different contributions to noise production are analyzed in Section 5.

2. FLOW CONFIGURATION AND NUMERICAL METHOD

We consider a 2D spatially developing plane compressible mixing layer between two parallel streams ($U_{\max}=1.6c$ and $U_{\min}=0.8c$ where c is the speed of sound) in a Cartesian frame of

Copyright © 2009 John Wiley & Sons, Ltd.

DOI: 10.1002/fld

reference (Oxy), where x and y are the streamwise and transverse directions, respectively, and (u, v) (or (u_1, u_2)) are the corresponding velocity components.

The whole computational domain size is $(L_x, L_y) = (75\delta_{\omega_0}, 50\delta_{\omega_0})$ corresponding to a Cartesian non-staggered computational grid with $(N_x, N_y) = (901, 601)$ points. δ_{ω_0} is the vorticity thickness of the velocity profile at the inlet plane $x = x_0$ (see Figure 1). All axis coordinates in the following figures are normalized with δ_{ω_0}, which provides a reference length for the large-scale coherent flow structures in the computational domain. Figure 1 displays the vorticity field superimposed on the far-field acoustic fluctuating pressure. Maxima levels of the fluctuating pressure field are about ± 600 Pa, which are small compared with the aerodynamic pressure fluctuations (around 10^5 Pa). In this figure, we also observe two directivities related to the convective effects in the high $(y>0)$ and low speed $(y<0)$ domains.

The part of the computational domain which will be investigated extends to $17\delta_{\omega_0}$ in the streamwise direction and from $-12.5\delta_{\omega_0}$ to $+12.5\delta_{\omega_0}$ in the transverse direction (Figure 1). It is observed in Figure 2 that in the target domain, $y \in [7\delta_{\omega_0}, 12\delta_{\omega_0}]$, the pressure intensity decays as $1/r$, corresponding to the far-field acoustic behaviour. This conclusion justifies the use of this domain to investigate the causality method between velocity field and the far-field acoustics.

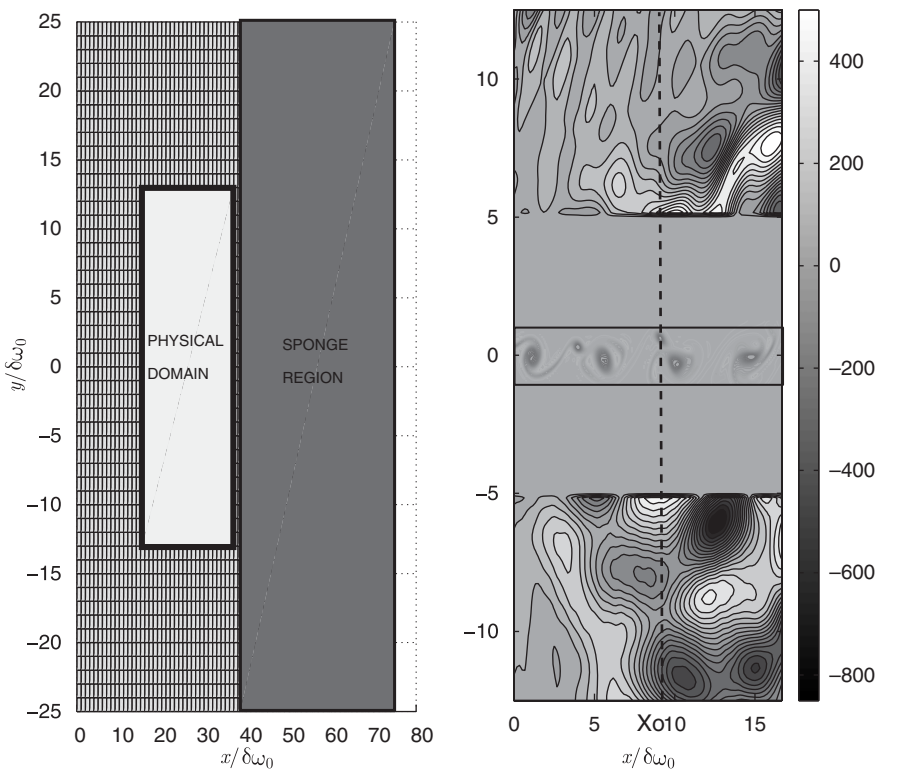

Figure 1. Left-hand side: whole computational domain. Right-hand side: vorticity field superimposed onto the far-field acoustic fluctuating pressure, extracted from the physical domain.

Copyright © 2009 John Wiley & Sons, Ltd.

DOI: 10.1002/fld

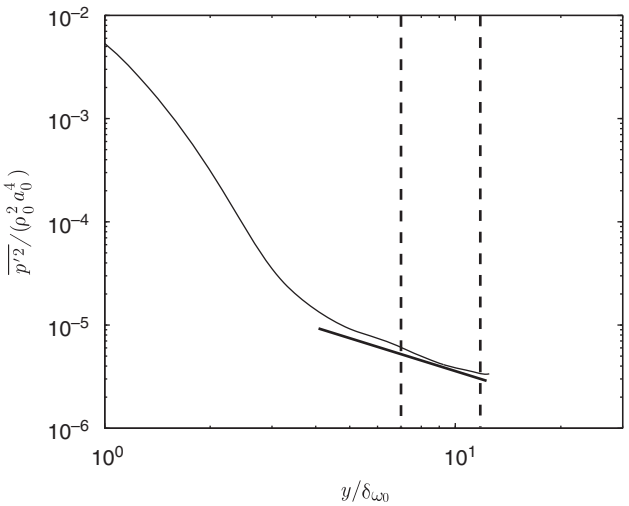

Figure 2. Sound intensity $\overline{p'^2}/(\rho_0^2 a_0^4)$ along a line at $x = 12\delta_{\omega_0}$, away from mixing layer flow ($y<0$). The line indicates a slope of -1. A log scale is used.

2.1. Numerical method

One of the main CAA problems consists in finding an efficient method for solving Navier–Stokes equations and/or Euler equations and to model the physical problems of interest. This last requirement involves the capability of defining boundary conditions that accurately represent the exact physical process while minimizing the computational cost and preserving the numerical stability. For that purpose, an in-house code solving these equations has recently been developed [22]. In the present work, the 2D inviscid compressible flow equations are formulated in Cartesian coordinates.

The numerical method is based on the pseudo-characteristic formulation of the convection terms introduced by Sesterhenn [23] and further developed by Lu and Sagaut [22]. This new decomposition of the pressure, velocity and entropy fluxes enables a very simple and natural use of upwind schemes to enforce numerical stability while minimizing the numerical dissipation. To enforce both numerical stability and accuracy for wave propagation problems, a high-order upwind dispersion relation preserving (DRP) scheme is used. In the interior nodes the fourth-order accurate upwind biased DRP scheme is used and this scheme is modified near the computational domain boundaries [22]. The time integration is performed using a third-order TVD Runge–Kutta scheme proposed by Shu and Osher [24].

The interest of the use of the pseudo-characteristic formulation is that it enables an easy implementation of efficient boundary conditions. Then, at outflow boundary, supersonic and subsonic non-reflecting boundary conditions are specified [22]. A sponge domain in the upstream direction (see Figure 1) is also implemented to damp the aerodynamic fluctuations before they reach the outlet plane, preventing occurence of spurious reflections. In practice, in this domain, the numerical scheme accuracy is decreased down to the first-order, so that the structures are not sustained. The sponge region is located downstream $x = 37\delta_{\omega_0}$ and dissipates vortices before other pairings happen downstream.

Copyright © 2009 John Wiley & Sons, Ltd.

DOI: 10.1002/fld

2.2. *Inflow forcing*

To make the mixing layer well defined and reproducible and to avoid any spurious self-excitation associated with the numerical discretization, it is forced with well-defined, unsteady deterministic harmonic perturbations associated with the mean hyperbolic inlet profile. The mixing layer is then forced at three frequencies: its fundamental frequency f_0 and its first two subharmonics $f_0/2$ and $f_0/4$. The fundamental frequency corresponds to the most amplified instabilities as predicted by the linear stability analysis of the inviscid hyperbolic tangent inlet profile [25]. The amplitude of the fundamental frequency is 0.001, whereas the amplitudes of the subharmonics are 0.0005. No phase shift was specified between each mode.

3. MATHEMATICAL TOOLS

In the following, POD and QSE mathematical tools are applied to the fluctuating quantities (velocity and pressure) only. These quantities are deduced from the classical Reynolds decomposition: $u_i = \overline{U_i} + u_i'$ and $p = \overline{P} + p'$, where the overbar denotes time average and u_i' and p' are the fluctuating velocity and pressure fields, respectively.

3.1. *Proper orthogonal decomposition (POD)*

POD was first proposed by Lumley [26] in 1967 as an objective technique for detecting and extracting coherent structures in a turbulent flow. According to Lumley, a coherent structure is the structure that has the largest mean square projection of the velocity field. This maximization leads to the definition of the following Fredholm integral eigenvalue problem [27]:

$$\sum_{j=1}^{N_c} \int_{\mathscr{D}} \overline{u_i'(X)u_j'(X')}\Phi_j^{(n)}(X')\,\mathrm{d}X' = \lambda^{(n)}\Phi_i^{(n)}(X) \tag{1}$$

where X denotes the space variable (x, y), N_c is the total number of the velocity components taken into account and $\mathscr{D}$ is the spatial domain investigation. $R_{ij}(X', X) = \overline{u_i'(X)u_j'(X')}$ represents the time average two-point spatial correlation tensor. In this equation, $\Phi^{(n)}(X)$ are the spatial POD eigenfunctions and $\lambda^{(n)}$ the corresponding eigenvalues, respectively. The projection of the instantaneous velocity fields onto the POD eigenfunctions provides the POD temporal coefficients $a^{(n)}(t)$. These elements define the classical POD method. Particular POD applications lead to an integral eigenvalue problem, which quickly overcomes the available computer capabilities. To alleviate this problem, Sirovich [28] developed a snapshot method that allows for a drastic reduction of the order of the POD eigenfunction problem (see also Holmes *et al.* [27]). In the snapshot method, the Fredholm integral eigenvalue problem is then computed from the $R_{ij}(t, t')$ correlation tensor based on a spatial average. Such a problem leads to the definition of temporal POD eigenfunctions $a^{(n)}(t)$, which are choosen to be orthonormal $\overline{a^{(n)}(t)a^{(m)}(t)} = \delta_{nm}$, with δ the Kronecker symbol. Each POD coefficient $\Phi^{(n)}(X)$ is then deduced from the projection of the instantaneous velocity field onto the POD eigenfunction $a^{(n)}(t)$. These coefficients are uncorrelated and $\langle \Phi^{(n)}\Phi^{(m)} \rangle = \lambda^{(n)}\delta_{nm}$, where $\langle\rangle$ is related to the spatial average. The instantaneous fluctuating

Copyright © 2009 John Wiley & Sons, Ltd.

DOI: 10.1002/fld

velocity component u_i is then expressed as follows

$$u_i(X,t)=\sum_{n=1}^{N_{\mathrm{mod}}} a^{(n)}(t)\Phi_i^{(n)}(X) \tag{2}$$

where N_{mod} is the total number of the POD modes.

Because we want to extract coherent events associated with the main source of noise emission, we propose to decompose the fluctuating velocity field into three parts, namely: large-scale coherent structure (LCS), small-scale coherent structures (SCS) and background incoherent fluctuations, respectively. Each flow contribution is defined, thanks to the POD decomposition. Since this decomposition is based on the two-point correlation tensor, which is a statistical quantity computed from all types of flow structures, isolated instantaneous structures (e.g. vortices, shear layers) and events (advection of coherent structures, merging of vortices) are not represented by a single POD mode and therefore has a non-local signature on POD basis. In the same way, such structures are related to broadband spectra on non-local bases like the Fourier basis. Similar POD decompositions have been already used to extract the mean part, coherent part and background fluctuations of turbulent flows [29, 30]. In these previous works, the background fluctuations were supposed to be QG. Following these preliminary works, we propose to define and extract background velocity fluctuations as the residual field in the POD decomposition, which exhibit QG properties. In practice, this is done looking at their probability density function (PDF) and the corresponding skewness and flatness factors that have to be close to 0 and 3, respectively (see Section 4). The origin of this Gaussian contribution is still an open issue and may be interpreted in different ways. It is important to note that similar results have been obtained using experimental data in very different flow configurations (Hot Wire Anemometry database [29] or Particle Image Velocimetry database [30]). First, it might be linked to residual eigenmodes related to low-energy numerical or measurement errors. The second possible explanation is that the Gaussian has a physical origin. It is worth recalling here that the Wavelet decomposition has been observed to enable the identification of a significant Gaussian contribution in strongly organized 2D turbulent fields [31, 32]. This feature remains to be understood, as the possible occurence of a universal slope in the POD spectrum in turbulent flows.

Finally, the instantaneous fluctuating velocity component u_i is decomposed as follows:

$$u_i'(X,t)=u_i^{\mathrm{LCS}}(X,t)+u_i^{\mathrm{SCS}}(X,t)+u_i^{\mathrm{QG}}(X,t) \tag{3}$$

Each component can then be expressed as a summation of POD modes:

$$u_i^{\mathrm{LCS}}(X,t)=\sum_{n=1}^{N_1} a^{(n)}(t)\Phi_i^{(n)}(X) \tag{4}$$

$$u_i^{\mathrm{SCS}}(X,t)=\sum_{n=N_1+1}^{N_2-1} a^{(n)}(t)\Phi_i^{(n)}(X) \tag{5}$$

$$u_i^{\mathrm{QG}}(X,t)=\sum_{n=N_2}^{N_{\mathrm{mod}}} a^{(n)}(t)\Phi_i^{(n)}(X) \tag{6}$$

The problem associated with such a POD flow splitting consists in adequately determining the parameters N_1 and N_2. Details of the determination procedure are given below.

Copyright © 2009 John Wiley & Sons, Ltd.

DOI: 10.1002/fld

3.2. Quadratic stochastic estimation (QSE)

SE has been first introduced in the field of turbulence research by Adrian [33] who proposed to estimate the flow behaviour using a particular condition referred to as a conditional eddy. This conditional eddy can be estimated using various quantities and multiple SE applications have been already performed [34–38]. This approach was successfully used to approximate conditional averages and to identify and describe coherent motions of turbulent flows [34–36]. Generally, the Linear version of the SE (LSE) provides satisfactory conditional averages of the LCS present in turbulent flows [34, 36]. The higher-order (larger than 1) terms seem to have little influence in the large-scale pattern of the flow [39]. Nevertheless, this linear form corresponds to a maximum likelihood estimate of the stochastic model parameters if the deviations of data from the estimate are independent and follow a normal distribution [40]. The condition of joint normalcy between turbulent data and event measures is not generally satisfied (see Section 4). Therefore, many works have provided a physical rationale for preferentially using the QSE procedure instead of LSE [19, 35, 38]. The inclusion of non-linear terms in the SE model may be viewed as recognition that real distributions of turbulent data and event vectors are not jointly normal. Moreover, when dealing with two variables (velocity and pressure fields), the use of QSE leads to quantitatively more accurate results than those deduced from LSE [19, 38]. Based on these preliminary works and also on the fact that the far-field pressure is correlated with the square of the velocity amplitude fluctuations [41], QSE is used in the present work to estimate the far-field acoustic pressure from the knowledge of selected aerodynamic coherent events. Note that additional comments are provided in Section 4 justifying the preferential use of QSE.

Mathematical formulation

Let us asssume that the aerodynamic events can be represented with the following instantaneous u_i^{LCS} (or u_i^{SCS}) vector field available at N_{ref} locations. For the sake of simplicity, the time dependency will be omitted in the equations below. At a given location X' in the far acoustic field region, the QSE estimation of the pressure $p'(X')$ is expressed as a function of the known $u_i^{\mathrm{LCS}}(X_{\mathrm{ref}})$ (or u_i^{SCS}) velocity field, which is available inside the flow at N_{ref} reference locations

$$p_{\mathrm{qse}}^{\mathrm{LCS}}(X') = A_i^p(X', X_{\mathrm{ref}})u_i^{\mathrm{LCS}}(X_{\mathrm{ref}}) + A_{jk}^p(X', X_{1\mathrm{ref}}, X_{2\mathrm{ref}})u_j^{\mathrm{LCS}}(X_{1\mathrm{ref}})u_k^{\mathrm{LCS}}(X_{2\mathrm{ref}}) \tag{7}$$

using the notation of repeated indices. The determination of the coefficients $A_i^p(X', X_{\mathrm{ref}})$ and $A_{jk}^p(X', X_{1\mathrm{ref}}, X_{2\mathrm{ref}})$ is based on the minimization of the mean square error in the estimate. A linear system of equations is then obtained, allowing the determination of these coefficients as a function of the two and three point spatial correlations tensor $\overline{p'(X')u_i^{\mathrm{LCS}}(X_{\mathrm{ref}})}$ and $\overline{p'(X')u_i^{\mathrm{LCS}}(X_{1\mathrm{ref}})u_j^{\mathrm{LCS}}(X_{2\mathrm{ref}})}$. The computation of these coefficients which is time independent is similar to the one proposed by Murray and Ukeiley [37].

4. POD AND QSE ANALYSES

4.1. POD application

The POD modes are computed using $N_t = 900$ (2D) instantaneous velocity snapshots obtained by performing the direct numerical simulation of the compressible mixing layer flow. The two velocity

Copyright © 2009 John Wiley & Sons, Ltd.

DOI: 10.1002/fld

components are stored every 30 time steps, in a specific flow subdomain in which acoustic sources will be determined. This subdomain is located inside the shear flow region: $([X_{\text{ref}}];[Y_{\text{ref}}])=([3\delta_{\omega_0}:12\delta_{\omega_0}];[-1.1\delta_{\omega_0}:1.1\delta_{\omega_0}])$ corresponding to a regular mesh of $(n_x\times n_y)=(109\times 29)$ points. It is represented with a black box in Figure 6. The full snapshot set correspond to the passage of more than 120 large-scale structures, allowing for the computation of converged statistics.

The 2D fluctuating velocity field represented by a matrix function: $\mathbf{V}(X_{ij},t_k)$, $i=1,\ldots,n_x$, $j=1,\ldots,n_y$, $k=1,\ldots,N_t$ is retained. It is assumed to form a linear infinite dimensional Hilbert space on a spatial domain $n_x\times n_y$. The implementation of the snapshot POD procedure applied to numerical data yields the definition of $(N_{\text{mod}}=N_t)$ POD eigenfunctions, $a^{(n)}(t)$. Figure 3 shows the convergence of the POD accumulated eigenvalues. A large part of the turbulent energy is then concentrated in a few primary modes due the high coherence level of the flow. For instance, the first 5 and 50 POD eigenfunctions among the 900 available ones, capture 90% and more than 99% of the total energy, respectively.

Based on this flow decomposition, a first analysis is performed to extract coherent structures (LCS and SCS fields) and background incoherent fluctuations. To determine the N_2 parameter, which defines the separation between coherent and incoherent flow contributions (see Equation (6)), the properties of the incoherent fluctuations are investigated. First, an analysis of the associated skewness S and flatness T coefficients is performed. A parametric study of these coefficients versus N_2 is done. Figure 4 displays the evolution of the spatially averaged skewness coefficients computed from background fluctuations, $\langle S_{u_i}^{\text{QG}}\rangle$. We then observe that both $\langle S_{u_1}^{\text{QG}}\rangle$ and $\langle S_{u_2}^{\text{QG}}\rangle$ coefficients converge towards zero for $N_2>90$. Quasi-similar results are obtained for the spatially averaged flatness coefficients. In a second step, an analysis of the PDF associated with the background fluctuations is performed as a function of N_2. An illustration is given in Figure 5 for $N_2=100$, where the PDFs of the transverse velocity component extracting from background QG fluctuations

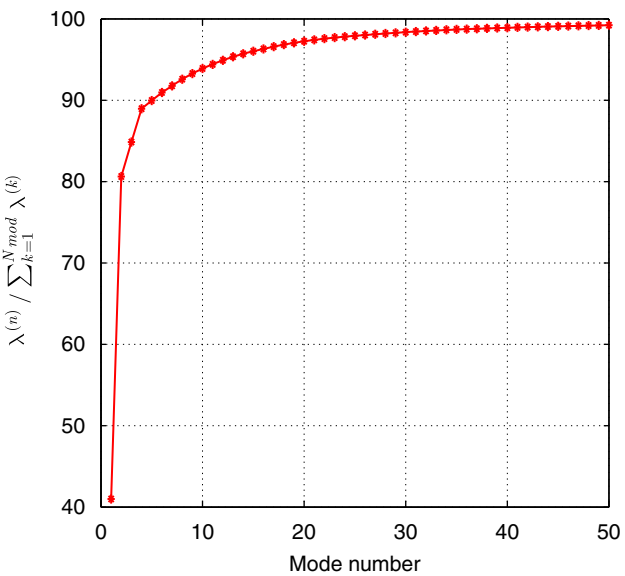

Figure 3. POD convergence analysis. x-axis is limited to 50 among the 900 available modes.

Copyright © 2009 John Wiley & Sons, Ltd.

DOI: 10.1002/fld

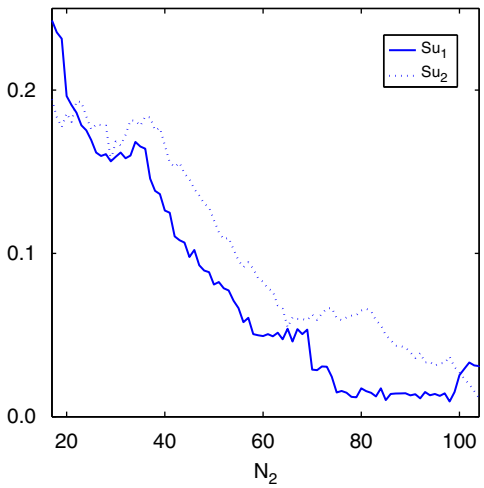

Figure 4. Evolution of the spatially averaged skewness $\langle S_{u_i}^{QG} \rangle$ coefficients versus N_2.

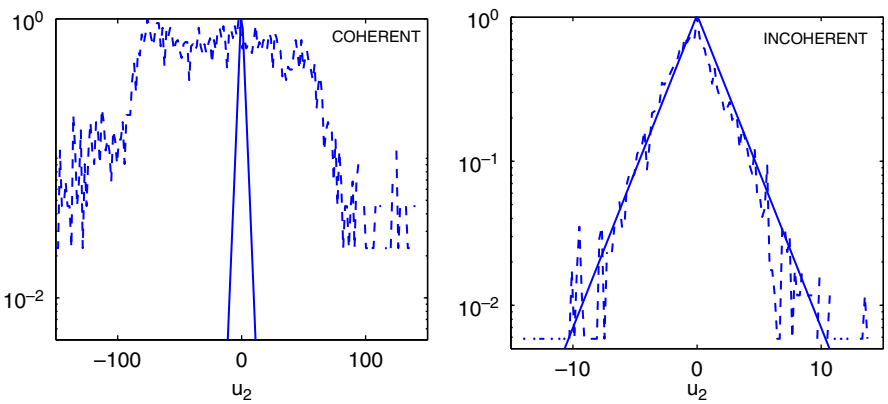

Figure 5. Comparative analysis of the normalized PDF of transverse velocity component (dashed line). Left-hand side: coherent field, including both LCS and SCS fields; Right-hand side: incoherent background fluctuations. The solid line corresponds to a Gaussian fit.

and also from the coherent field are plotted. The PDF of the incoherent velocity is similar to the one of a Gaussian variable. Conversely, the PDF of the coherent velocity greatly differs from the Gaussian one. Otherwise, note that when N_2 values are in [90 : 110] interval, we do not observe significant differences on skewness and flatness coefficients and on the PDF representation. N_2 is then choosen to be equal to 100. The coherent flow including both LCS and SCS fields is then reconstructed from 11% of the total number of POD modes and these POD modes correspond to 99.8% of the total fluctuating kinetic energy. Moreover, the QG background fluctuations are computed from 89% of the total number of POD modes and retain only 0.2% of the total kinetic

Copyright © 2009 John Wiley & Sons, Ltd.

DOI: 10.1002/fld

energy. Owing to the fact that QG fluctuations correspond to a very small flow energy contribution, these fluctuations can be sensitive to numerical errors as well as to the flow background fluctuations.

These results are quite similar to previous ones based on wavelet flow decomposition applied to a 2D isotropic turbulent flow [31].

The difficulty then arises in choosing the N_1 number according to the current objective, that is, to extract the part of the coherent motion that is implicated in the main noise emission. A discussion on choice of this number is performed in Section 5.1.

4.2. QSE analysis

An analysis of the fluctuating pressure and velocity fields is performed, justifying the preferential use of the QSE procedure versus LSE. Figure 6 presents the PDF obtained from the fluctuating u_1 velocity component inside the flow field and the fluctuating pressure in the far acoustic field

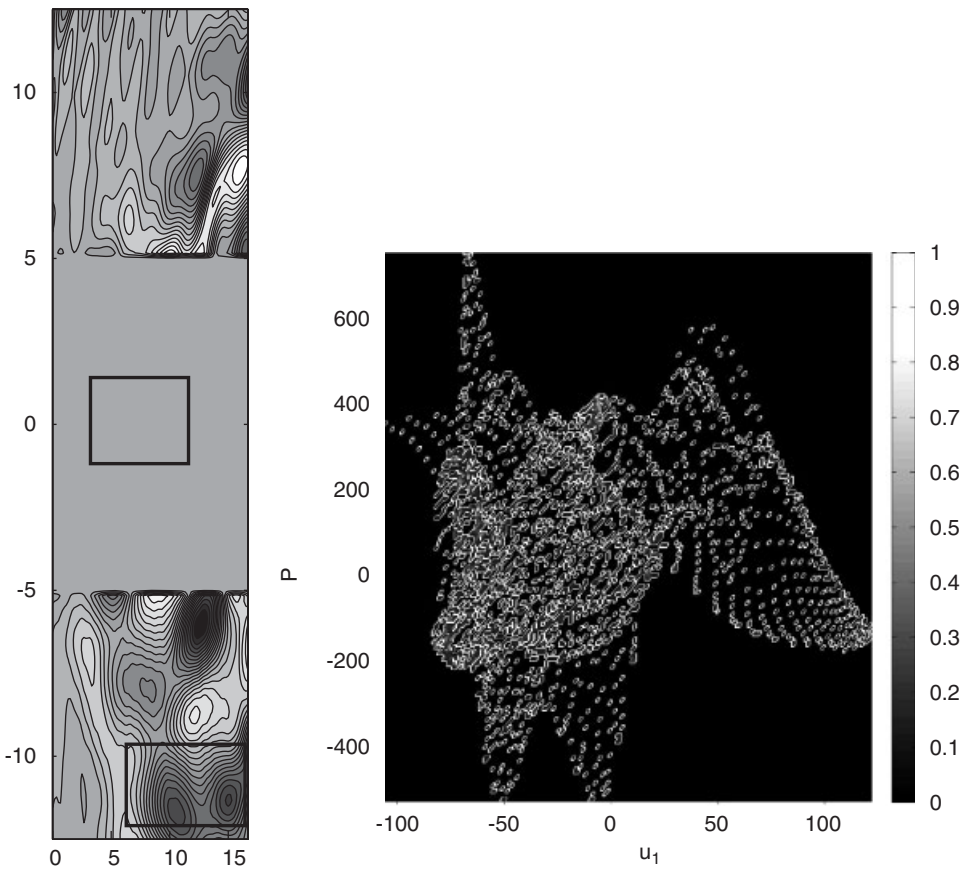

Figure 6. Left-hand side: extracted numerical domains (velocity field, inside the mixing layer flow and far-field acoustic pressure). Right-hand side: normalized PDF between u_1 velocity component (x-axis) and pressure field (y-axis) extracted from these domains.

Copyright © 2009 John Wiley & Sons, Ltd.

DOI: 10.1002/fld

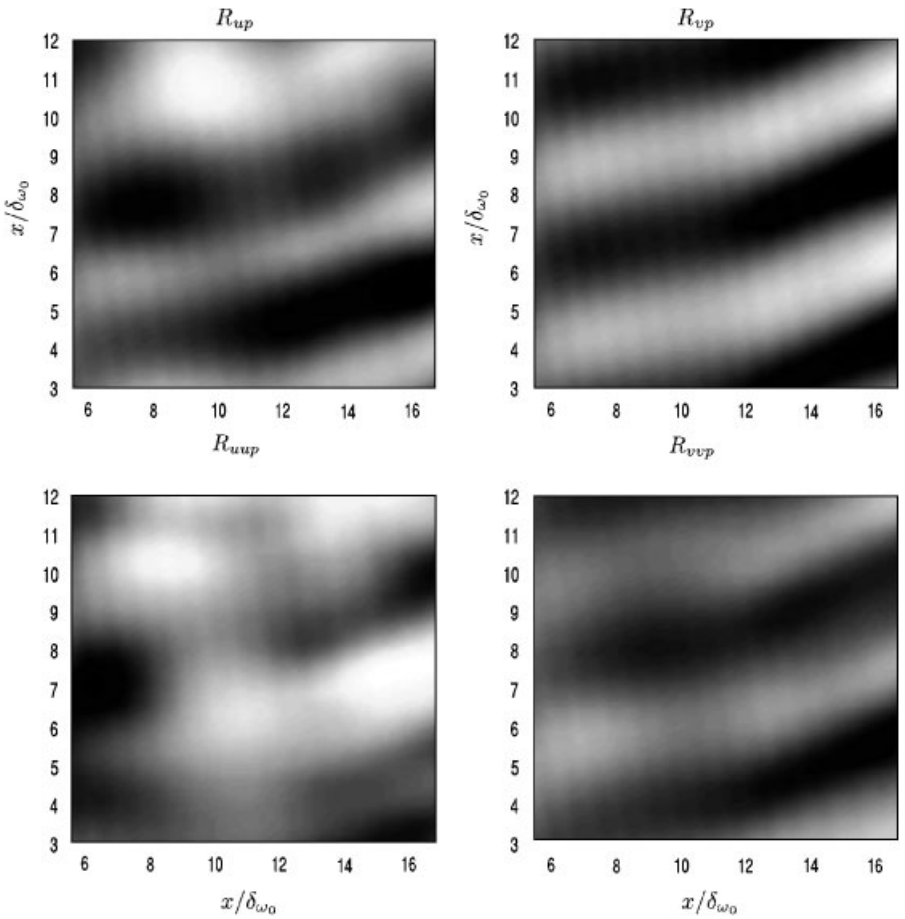

Figure 7. Two point spatial correlation tensor between velocity components (along the line $y=0$) and pressure field (along the line $y=-11\delta_{\omega_0}$). Range colour is $[-0.5, 0.6]$ in each figure.

(in the low-speed domain $y<-10\delta_{\omega_0}$). The computed PDFs greatly deviate from the Gaussian one, showing that (p, u_i) fields do not follow a normal distribution. Similar results are obtained when PDFs are computed from pressure field obtained in the high-speed domain ($y>8\delta_{\omega_0}$).

Moreover, Figure 7 displays the two and three points spatial correlation tensors $R_{ip}(X_{\text{ref}}, X')$ and $R_{ijp}(X_{1\text{ref}}, X_{2\text{ref}}, X')$. Such correlations are computed from velocity fields obtained in the core region of the plane mixing layer ($x\in[3\delta_{\omega_0}, 12\delta_{\omega_0}]$, $y=0$) and from pressure field obtained in the low-speed domain ($x\in[5.7\delta_{\omega_0}, 16.5\delta_{\omega_0}]$, $y=-11\delta_{\omega_0}$). The levels of two and three point correlations are quite similar, meaning that the influence of the higher-order terms on the SE procedure is not negligible. Similar results are obtained when computing these correlations from fluctuating pressure field obtained in the far high-speed domain. A brief analysis of these correlations shows that the far-field acoustic pressure is well correlated with the large-scale coherent flow structure. These figures also give an indication about the noise emission directivity. Indeed, the pressure

Copyright © 2009 John Wiley & Sons, Ltd.

DOI: 10.1002/fld

field is mainly correlated with the flow structures in the mixing layer flow, with a spatial decay of several δ_{ω_0}.

Finally, these analyses (PDF, two and three point correlations) justify the inclusion of the quadratic terms in the SE procedure.

5. RESULTS

The POD flow partitioning is first investigated. Then, the instantaneous far-field acoustic pressure is estimated using QSE from the knowledge of each instantaneous velocity field contribution inside the plane mixing layer flow. Note that for the QSE estimation of the pressure field, only (4×3) velocity samples among the $(n_x \times n_y)$ available ones are used as conditional events. These reference samples are located at $y=\pm\delta_{\omega_0}/2$ and $y=0$ in the y-direction and are equally spaced in the streamwise direction.

5.1. *POD flow partitionning*

The first step consists in determining the N_1 parameter, which defines the separation between the LCS and SCS of the flow. To this end, we compute the root mean square (RMS) of the QSE reconstructed pressure field, $p'^{\mathrm{rms}}_{\mathrm{qse}}$. This QSE reconstruction is performed from the knowledge of selected coherent events that are represented with a summation of POD modes (see Equations (4) and (5)). The influence of the velocity POD mode number N_1 on the RMS pressure field, $p'^{\mathrm{rms}}_{\mathrm{qse}}$ can then be investigated. Thanks to the foreknowledge of the full data set, the RMS field, $p'^{\mathrm{rms}}_{\mathrm{qse}}$, can be directly compared with the original one, $p'^{\mathrm{rms}}_{\mathrm{orig}}$, computed from raw numerical data. An investigation of the following error field

$$\mathrm{error}^{p'}_{\mathrm{rms}}(X') = \overline{p'^{\mathrm{rms}}_{\mathrm{orig}}(X')} - \overline{p'^{\mathrm{rms}}_{\mathrm{qse}}(X')} \tag{8}$$

is carried out. A spatial average of $\mathrm{error}^{p'}_{\mathrm{rms}}(X')$, denoted $\langle \mathrm{error}^{p'}_{\mathrm{rms}} \rangle$, is then computed in the far low-speed domain ($y<-7\delta_{\omega_0}$) and/or in the far high-speed domain ($y>7\delta_{\omega_0}$).

The LCS velocity field is then extracted using N_1 values pertaining to the interval [1:99]. For each extracted LCS field, the far-field acoustic pressure is QSE-estimated (Equation (7)). The spatial average of the resulting error field, $\langle \mathrm{error}^{p'}_{\mathrm{rms}} \rangle$, is then computed for each N_1 value. Figure 8 presents the evolution of $\langle \mathrm{error}^{p'}_{\mathrm{rms}} \rangle$ versus N_1, computed over the high ($y>7\delta_{\omega_0}$) and low ($y<-7\delta_{\omega_0}$) speed domains. Both figures exhibit similar behaviour. Notice that when N_1 is greater than 25, almost constant RMS error values of 0.02 and 0.015 are obtained in the high- and low-speed domains, respectively.

Another investigation of $\langle \mathrm{error}^{p'}_{\mathrm{rms}} \rangle$ versus N_1 is now performed, in which p' is now deduced from the QSE estimation using the SCS velocity field as conditional events. This SCS velocity field is computed from Equation (5) varying N_1 while keeping $N_2=100$. For each N_1 value, a QSE reconstruction of the far-field acoustic pressure is performed. The RMS error field, $\langle \mathrm{error}^{p'}_{\mathrm{rms}} \rangle$, is then computed for each N_1 value using a spatial average over the far high-speed domain (Figure 9). A similar representation of $\langle \mathrm{error}^{p'}_{\mathrm{rms}} \rangle$ is obtained in the low-speed domain. For $N_1=5$, the evolution of $\langle \mathrm{error}^{p'}_{\mathrm{rms}} \rangle$ exhibits a slight slope change. We also observe that for $N_1<10$, the RMS error values

Copyright © 2009 John Wiley & Sons, Ltd.

DOI: 10.1002/fld

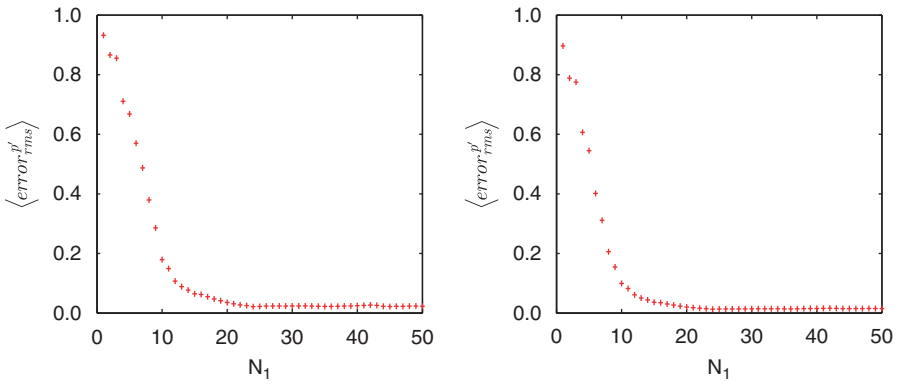

Figure 8. Evolution of $\langle \text{error}^{p'}_{\text{rms}} \rangle$ versus N_1 where p' is the reconstructed pressure field based on the LCS velocity field (Equation (4)). Left-hand side: the spatial average is performed in the far high-speed domain. Right-hand side: the spatial average is performed in the far low-speed domain.

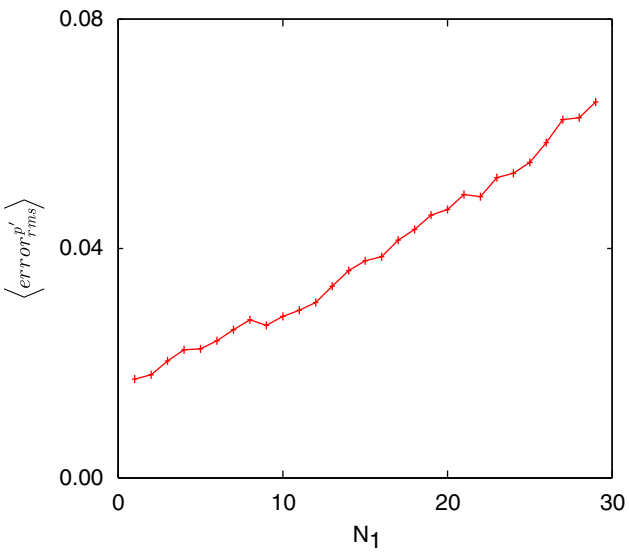

Figure 9. Evolution of $\langle \text{error}^{p'}_{\text{rms}} \rangle$ as a function of N_1 where p' is the reconstructed pressure field based on the SCS velocity field (Equation (5) with $(N_2 = 100)$). The spatial average is performed in the far high-speed domain.

are quite similar to the one using $N_1 = 1$. This result shows that the first POD velocity modes have no real effect on the far-field pressure estimated via the QSE procedure. In the same way, the LCS associated with these first POD modes have no significant contribution to the RMS of the pressure field. Finally, based on this result and also on the analysis of instantaneous vorticity fields associated with LCS and SCS velocity fields, respectively, N_1 is set equal to 5 in the following. Then, LCS field contain 90% of the total kinetic flow energy (see Figure 3), and SCS (SCS field,

Copyright © 2009 John Wiley & Sons, Ltd.

DOI: 10.1002/fld

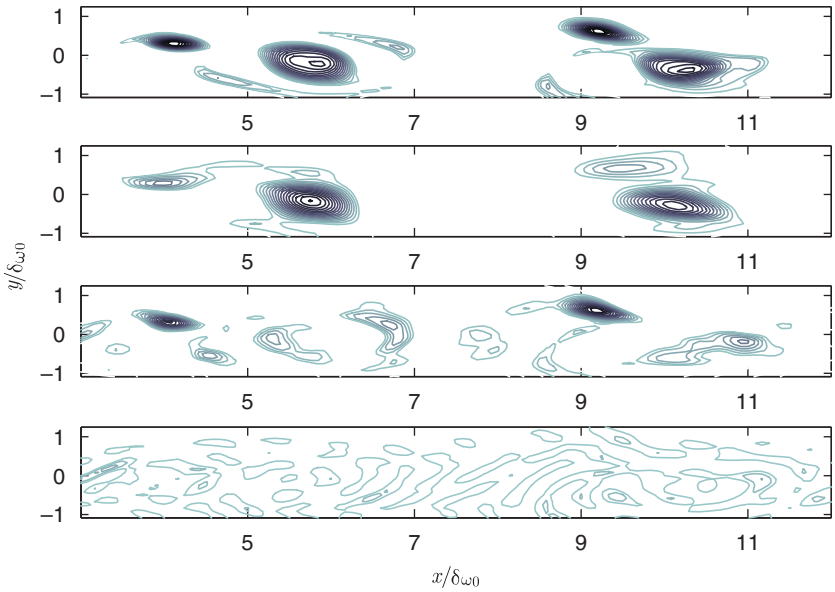

Figure 10. Illustration of the POD flow decomposition. Instantaneous vorticity field. Top to bottom: original field, LCS field, SCS field and quasi-Gaussian (QG) fluctuations. Contour lines are interval from −420 to −5 with a step of 20.

Equation (5) using $(N_1, N_2) = (5, 100)$) contributes to no more than 10% of the total turbulent kinetic flow energy.

Each 2D instantaneous velocity field is then decomposed into three parts: LCS and SCS coherent fields and background incoherent fluctuations (QG field). An illustration of this flow decomposition is given in Figure 10 in which instantaneous vorticity fields extracted from each part of this flow decomposition are provided. In this figure, LCS (LCS field) are well isolated from the first POD modes. SCS (SCS field) are also clearly identified. This SCS field contains the shear zones related to the LCS field.

5.2. QSE estimation of the far-field acoustic pressure

Based on the POD decomposition, resulting in LCS, SCS and QG velocity fields are then successively used as conditional events for the QSE estimation of the far-field acoustic pressure. First, an analysis is performed from the RSM values of the resulted pressure field. Second, a spectral analysis of the far-field acoustic pressure obtained at selected locations is carried out.

RMS of the far-field acoustic pressure

Figure 11 displays the RMS of the following pressure fields:

(a) Original pressure field directly obtained from the numerical simulation (reference data).
(b) p'_{qse}: QSE estimated pressure field using the N_{mod} POD velocity modes corresponding to the entire fluctuating velocity field as conditional event.
(c) $p^{\mathrm{LCS}}_{\mathrm{qse}}$: QSE estimated pressure field using the LCS field (corresponding to the 5 first POD modes) as conditional event.

Copyright © 2009 John Wiley & Sons, Ltd.

DOI: 10.1002/fld

(d) p_{qse}^{SCS}: QSE estimated pressure field using the SCS field (corresponding to the summation of POD modes from 6 to 99) as conditional event.
(e) p_{qse}^{QG}: QSE estimated pressure field using the QG fluctuations (corresponding to the residual POD modes) as conditional event.

Results of test case (b) are quite similar to the original data, making it possible to validate and to show the efficiency of the QSE estimation. Moreover, RMS values deduced from test case (b) are different from the summation of the ones arising from test cases (c), (d) and (e). This observation is directly linked to the fact that the QSE procedure takes into account the coupling existing between each velocity POD mode. Each flow contribution is phase correlated and then a partial cancellation occurs when dealing with the whole velocity field (test case b). Conversely, when using LSE procedure, such coupling cannot be taken into account [42].

This figure shows also that the LCS (LCS field) are not responsible for the main noise emissions especially in the low-speed domain ($y < -8\delta_{\omega_0}$). This result is in agreement with previous studies in which it has been observed that large-scale convective structures are not the essential features for the noise emission in turbulent shear flows. The main part of the noise emission is then related to the SCS events. According to Figure 10, this SCS field is composed of SCS that interacts with themselves and also of shear flow events that tend to modify the large-scale flow structures. It is then confirmed that the interaction between flow structures and especially between small-scale structures is the main aerodynamic mechanism for noise emission in shear flows.

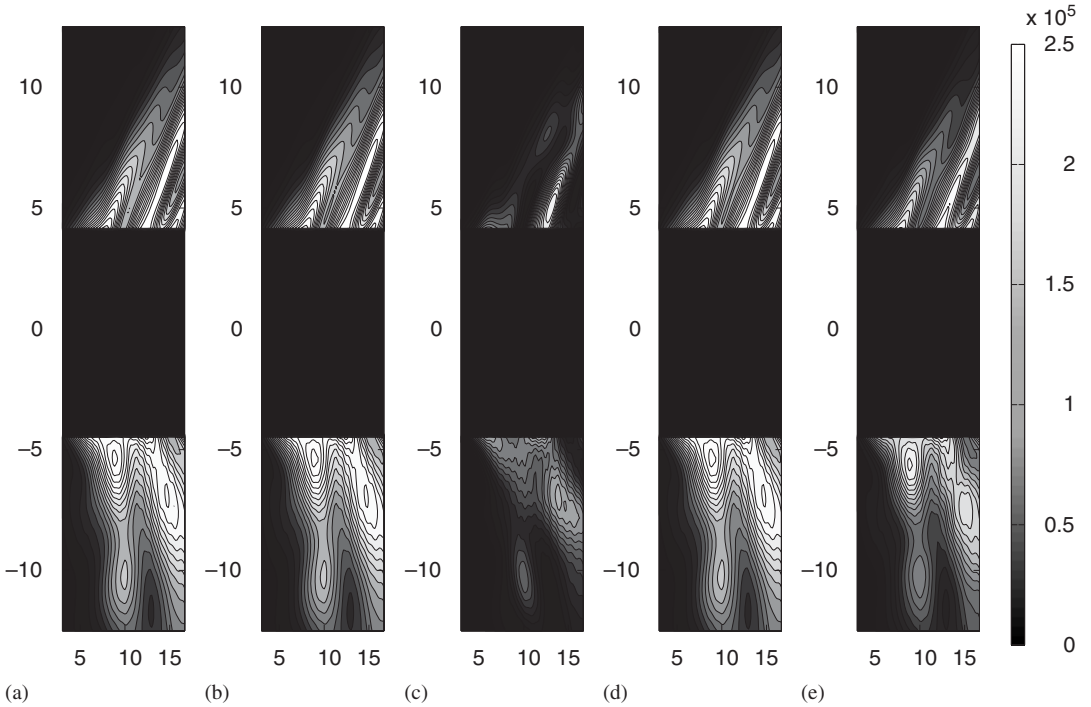

Figure 11. RMS of the fluctuating pressure field reconstructed from QSE using different conditional events. See in the text the corresponding test cases from (a) to (e). A same colormap is used.

Copyright © 2009 John Wiley & Sons, Ltd.

DOI: 10.1002/fld

Spectral analysis of the far-field acoustic pressure

A second analysis is performed to access the spectral content of the far-field pressure. Two selected locations, X_1 and X_2, are investigated. These points have the following coordinates $(x_1, y_1) = (15\delta_{\omega_0}, 6.5\delta_{\omega_0})$ in the high-speed domain and $(x_2, y_2) = (15\delta_{\omega_0}, -7\delta_{\omega_0})$ in the low-speed domain. The temporal spectra are computed from the following reconstructed pressure fields: $p_{\text{qse}}^{\text{LCS}}$, $p_{\text{qse}}^{\text{SCS}}$ and $p_{\text{qse}}^{\text{GS}}$. Obtained spectra are compared with the original one deduced from raw numerical data. Figures 12 and 13 represent the pressure spectra obtained at X_1 and X_2, respectively. Original spectra in both supersonic and subsonic flow domain exhibit selected frequencies that are directly related to the combination of the fundamental frequency f_0 and its subharmonics of the plane mixing layer flow. Two frequency peaks are mainly obtained for $f_0/4$ and f_0 frequencies. The summation of the spectra associated with $p_{\text{qse}}^{\text{LCS}}$, $p_{\text{qse}}^{\text{SCS}}$ and $p_{\text{qse}}^{\text{GS}}$ pressure fields differs greatly from the original data due to the existence of a coupling between velocity POD modes, at it was previously noted. This can be explained by the fact that, when dealing with the full velocity field as a conditional event, some noise emission mechanisms may be partially cancelled by interactions between the three flow components, since they are not phase-locked.

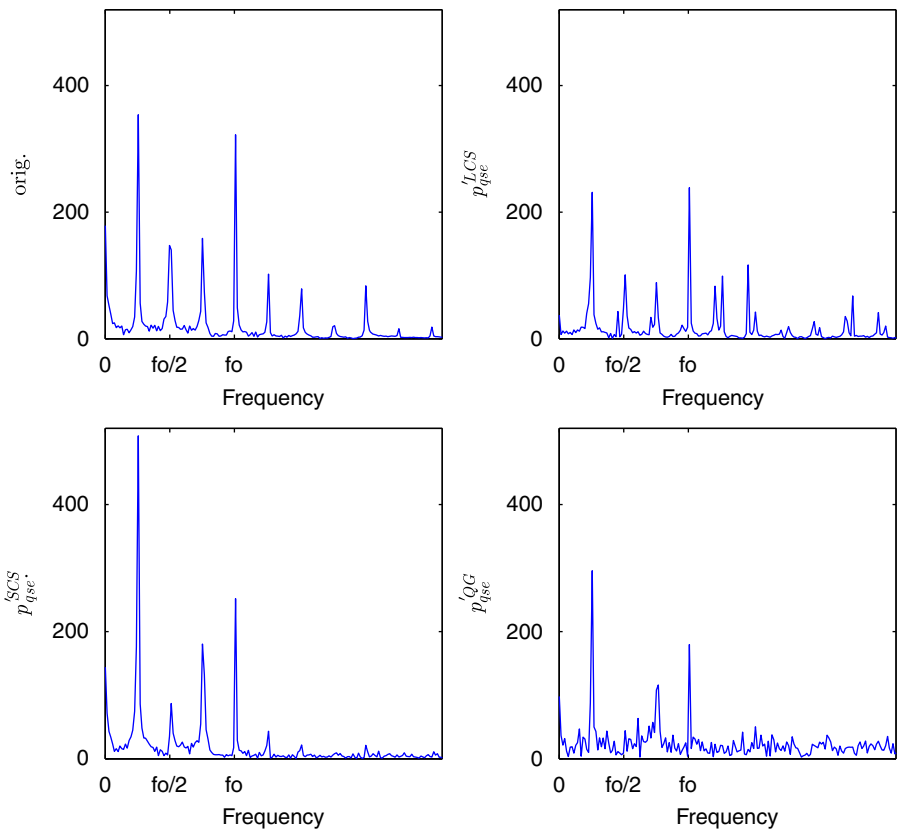

Figure 12. Spectra computed from $p_{\text{qse}}^{\text{LCS}}$, $p_{\text{qse}}^{\text{SCS}}$ and $p_{\text{qse}}^{\text{GS}}$ pressure fields, respectively, and compared with the original one. Spectra are computed at X_1, located in the high-speed domain.

Copyright © 2009 John Wiley & Sons, Ltd.

DOI: 10.1002/fld

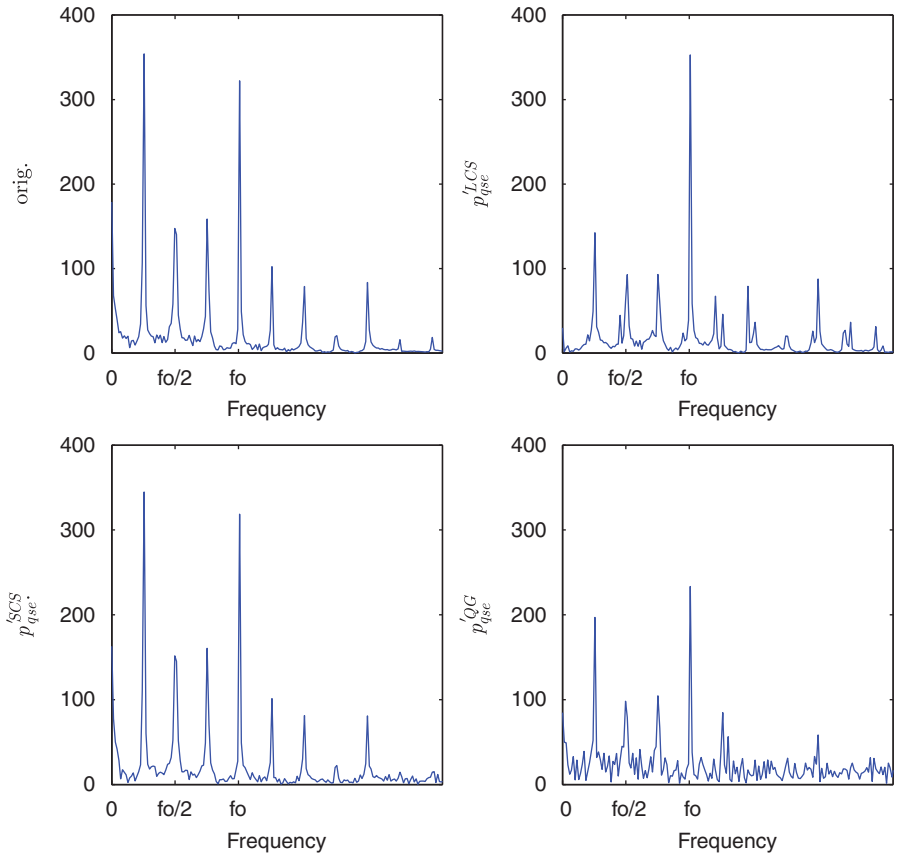

Figure 13. Spectra computed from $p_{\text{qse}}^{\text{LCS}}$, $p_{\text{qse}}^{\text{SCS}}$ and $p_{\text{qse}}^{\text{GS}}$ pressure fields, respectively, and compared with the original one. Spectra are computed at X_2 located in the low-speed domain.

In Figure 13, the $p_{\text{qse}}^{\text{SCS}}$ pressure spectrum clearly restores the original spectrum where obtained peaks have the same amplitudes as the original ones. This result confirms that for subsonic shear flow, most of the noise emission is due to the SCS. Conversely, the $p_{\text{qse}}^{\text{LCS}}$ pressure spectrum exhibits only the peak associated with the f_0 frequency, which corresponds to the passage of the large-scale flow structures. In Figure 12, the spectrum computed from the $p_{\text{qse}}^{\text{LCS}}$ pressure field exhibits similar peaks as the original pressure spectrum but with lower amplitudes. The spectrum computed from the $p_{\text{qse}}^{\text{SCS}}$ is quite similar to the original one even if the peak obtained at the frequency $f_0/4$ has a greater amplitude than the one obtained from the original data. In the high-speed domain, supersonic convective large-scale flow structures as well as the interactions between small-scale flow structures are involved in the noise emission. This last result is directly related to the non-localness of the aerodynamic events on the POD basis. The pairing process, which is known to be the main contributor to noise generation in the present flow, appears as a linear combination of a large number of POD modes. Therefore, acoustic wave generation involves all flow parts.

Copyright © 2009 John Wiley & Sons, Ltd.

DOI: 10.1002/fld

6. CONCLUSION

A new methodology based on an efficient coupling of proper orthogonal decomposition (POD) and stochastic estimation (SE) is developed to identify the essential aerodynamic mechanism involved in noise production by a plane mixing layer flow. This methodology is based on a judicious use of the flow statistics, and especially of the spatial velocity/velocity and velocity/pressure correlation tensors. Thus, POD is first used to decompose the instantaneous velocity field into several flow contributions. It then permits to isolate the large-(LCS) and small-scale coherent flow structure (SCS) and also some background Quasi-Gaussian (QG) fluctuations. The quadratic stochastic estimation (QSE) is implemented to estimate the far-field acoustic pressure associated with each flow component. By analyzing the RMS of the far-field acoustic pressure and also the associated spectra of the pressure field, we show that the main part of the noise emission is related to the SCS event of the plane mixing layer flow. Obtained results confirm the previous ones based on other methodologies applied to unbounded turbulent flows. Current methodology also confirms that in unbounded shear flows, several noise generation mechanisms occur as a function of individual aerodynamic contribution related to the large- and small-scale coherent flow structures and to the background fluctuations. Finally, such a POD/QSE combination, which allows for the reduction of the essential aerodynamic events that are involved in the main noise emission mechanisms, offers many prospectives for the problem of noise generation for unsteady unbounded turbulent flows. Indeed, based on this POD flow decomposition, it may be possible to improve the noise source modelling related to both LCS and SCS present in turbulent flows. Moreover, a subsequent analysis has to be performed in order to correlate the theoretical source noise emission and the flow event contribution detected from POD application.

REFERENCES

1. Lighthill MJ. On sound generated aerodynamically: I general theory. *Proceedings of the Royal Society of London* 1952; **211**:564–587.
2. Tam CKW. Computational aeroacoustic examples showing the failure of the acoustic analogy theory to identify the correct noise sources. *Journal of Computational Acoustics* 2002; **10**(4):387–405.
3. Peake N. A note on 'computational aeroacoustic examples showing the failure of the acoustic analogy theory to identify the correct noise sources' by CKW Tam. *Journal of Computational Acoustics* 2004; **12**(4):631–634.
4. Spalart RP. Application of full and simplified acoustic analogies to an elementary problem. *Journal of Fluid Mechanics* 2007; **578**:113–118.
5. Colonius T, Lele SK, Moin P. Sound generation in a mixing layer. *Journal of Fluid Mechanics* 1997; **330**:375–409.
6. Avital EJ, Sandham ND, Luo KH. Mach wave radiation by mixing layers. Part I: analysis of the sound field. *Theoretical and Computational Fluid Dynamics* 1998; **12**(2):73–90.
7. Bogey C, Bailly C, Juvé D. Numerical simulation of sound generated by vortex pairing in a mixing layer. *AIAA Journal* 2000; **40**(2):235–243.
8. Fortuné V, Lamballais E, Gervais Y. Noise radiated by a non-isothermal, temporal mixing layer. Part I: direct computation and prediction using compressible DNS. *Theoretical and Computational Fluid Dynamics* 2004; **18**(1):61–81.
9. Panda J, Seasholtz RG, Elam KA. Investigation of noise sources in high-speed jets via correlation measurements. *Journal of Fluid Mechanics* 2005; **537**:349–385.
10. Tinney CE, Coiffet F, Delville J, Hall AM, Jordan P, Glauser MN. On spectral linear stochastic estimation. *Experiments in Fluids* 2007; **41**(5):763–775.
11. Bogey C, Bailly C. An analysis of the correlations between the turbulent flow and the sound pressure fields of subsonic jets. *Journal of Fluid Mechanics* 2007; **583**:71–91.

Copyright © 2009 John Wiley & Sons, Ltd.

DOI: 10.1002/fld

12. Jordan P, Gervais Y. Subsonic jet aeroacoustics: associating experiment, modelling and simulation. *Experiments in Fluids* 2008; **44**(1):1–21.
13. Babucke A, Kloker M, Rist U. DNS of a plane mixing layer for the investigation of sound generation mechanisms. *Computers and Fluids* 2008; **37**(4):360–368.
14. Freund JB. Noise sources in a low-Reynolds-number turbulent jet at Mach 0.9. *Journal of Fluid Mechanics* 2001; **438**:277–305.
15. Ffwocs Williams JE, Kempton AJ. The noise from the large-scale structure of a jet. *Journal of Fluid Mechanics* 1978; **84**:673–694.
16. Jung D, Gamard S, George WK. Downstream evolution of the most energetic modes in a turbulent axisymmetric jet at high Reynolds number. Part 1. The near-field region. *Journal of Fluid Mechanics* 2004; **514**:173–204.
17. Bonnet JP, Cole DR, Delville J, Glauser MN, Ukeiley LS. Stochastic estimation and proper orthogonal decomposition: complementary techniques for identifying structure. *Experiments in Fluids* 1994; **17**:307–314.
18. Taylor JA, Glauser MN. Towards practical flow sensing and control via POD and LSE based low-dimensional tools. *Journal of Fluids Engineering* 2004; **126**(3):337–345.
19. Murray N, Ukeiley L. Modified quadratic stochastic estimation of resonating subsonic cavity flow. *Journal of Turbulence* 2007; **8**(53):1–23.
20. Hudy LM, Naguib A, Humphreys WM. Stochastic estimation of a separated-flow field using wall-pressure-array measurements. *Physics of Fluids* 2007; **19**:024103.
21. Picard C, Delville J. Pressure velocity coupling in a subsonic round jet. *International Journal of Heat and Fluid Flow* 2000; **21**(3):359–364.
22. Lu SY, Sagaut P. Pseudo-characteristic formulation and dynamic boundary conditions for computational aeroacoustics. *International Journal for Numerical Methods in Fluids* 2007; **53**(2):201–227.
23. Sesterhenn J. A characteristic-type formulation of the Navier–Stokes equations for high order upwind schemes. *Computers and Fluids* 2001; **30**:37–67.
24. Shu CW, Osher S. Efficient implementation of essentially non-oscillatory shock capturing schemes. *Journal of Computational Physics* 1989; **83**:32–78.
25. Monkewitz PA, Huerre P. The influence of the velocity ratio on the spatial instability of mixing layers. *Physics of Fluids* 1982; **25**:1137–1143.
26. Lumley JL. The structure of inhomogeneous turbulent flows. In *Atmospheric Turbulence and Radio Wave Propagation*, Yaglom AM, Tatarsky VI (eds). 1967; 166–178.
27. Holmes P, Lumley JL, Berkooz G. Turbulence, coherent structures, dynamical systems and symmetry. *Cambridge Monograph on Mechanics*, 1996.
28. Sirovich L. Turbulence and the dynamics of coherent structures. Part I: coherent structures. *Quaterly of Applied Mathematics* 1987; **XLV**:561–571.
29. Druault Ph, Delville J, Bonnet JP. Proper orthogonal decomposition of the mixing layer flow into coherent structures and turbulent Gaussian fluctuations. *Comptes Rendus Mécanique* 2005; **333**:824–829.
30. Roudnitzky S, Druault Ph, Guibert Ph. Proper orthogonal decomposition of in-cylinder engine flow into mean component, coherent structures and random Gaussian fluctuations. *Journal of Turbulence* 2006; **7**(70):1–19.
31. Farge M, Schneider K, Kevlahan N. Non-Gaussianity and coherent vortex simulation for two-dimensional turbulence using an adaptative orthogonal wavelet basis. *Physics of Fluids* 1999; **11**(8):2187–2201.
32. Farge M, Schneider K, Pelligrino G, Wray A, Rogallo R. Coherent vortex extraction in three dimensional homogeneous turbulence: comparison between CVS-wavelet and POD-Fourier decompositions. *Physics of Fluids* 2003; **15**:2886–2896.
33. Adrian RJ. On the role of conditional averages in turbulence theory. In *The 4th Biennial Symposium on Turbulence in Liquids*, Zakin J, Patterson G (eds). Science Press: Princeton, 1977; 322–332.
34. Adrian RJ, Jones BJ, Chung MK, Hassan Y, Nithianandan CK, Tung ATC. Approximation of turbulent conditional averages by stochastic estimation. *Physics of Fluids* 1989; **1**(6):992–998.
35. Brereton GJ. Stochastic estimation as a statistical tool for approximating turbulent conditional averages. *Physics of Fluids* 1992; **4**(9):2046–2054.
36. Druault Ph, Delville J, Bonnet JP. Experimental 3D analysis of the large scale behaviour of a plane turbulent mixing layer. *Flow Turbulence and Combustion* 2005; **74**(2):207–233.
37. Murray N, Ukeiley L. Estimation of the flow field from surface pressure measurements in an open cavity. *AIAA Journal* 2003; **41**(5):969–972.
38. Naguib AM, Wark CE, Juckenhofel O. Stochastic estimation and flow sources associated with surface pressure events in a turbulent boundary layer. *Physics of Fluids* 2001; **13**(9):2611–2626.

Copyright © 2009 John Wiley & Sons, Ltd.

DOI: 10.1002/fld

39. Tung T, Adrian R. Higher order estimates of conditional eddies in isotropic turbulence. *Physics of Fluids* 1980; **23**(7):1469–1470.
40. Papoulis A. *Probability Random Variables*, *and Stochastic Processes* (International Student edn). McGraw-Hill Kogakusha: Tokyo, 1965.
41. Laufer J, Yen TA. Noise generation by a low-Mach-number jet. *Journal of Fluid Mechanics* 1983; **134**:1–31.
42. Boree J. Extended proper orthogonal decomposition: a tool to analyse correlated events in turbulent flows. *Experiments in Fluids* 2003; **35**:188–192.

Copyright © 2009 John Wiley & Sons, Ltd.

DOI: 10.1002/fld